EUKARYOTIC CELL, May 2011, p. 683–695 Vol. 10, No. 5
1535-9778/11/$12.00 doi:10.1128/EC.00280-10
Copyright © 2011, American Society for Microbiology. All Rights Reserved.

Traffic of Chitin Synthase 1 (CHS-1) to the Spitzenkörper and Developing Septa in Hyphae of *Neurospora crassa*: Actin Dependence and Evidence of Distinct Microvesicle Populations[▽]†

Eddy Sánchez-León,[1] Jorge Verdín,[1] Michael Freitag,[2] Robert W. Roberson,[3] Salomon Bartnicki-Garcia,[1] and Meritxell Riquelme[1]*

Department of Microbiology, Center for Scientific Research and Higher Education of Ensenada (CICESE), Ctra. Ensenada-Tijuana No. 3918, Ensenada, Baja California, C.P. 22860, Mexico[1]; Department of Biochemistry and Biophysics, Center for Genome Research and Biocomputing, Oregon State University, Corvallis, Oregon 97331-7305[2]; and School of Life Sciences, Arizona State University, Tempe, Arizona 85287[3]

Received 2 November 2010/Accepted 26 January 2011

We describe the subcellular location of chitin synthase 1 (CHS-1), one of seven chitin synthases in *Neurospora crassa*. Laser scanning confocal microscopy of growing hyphae showed CHS-1–green fluorescent protein (GFP) localized conspicuously in regions of active wall synthesis, namely, the core of the Spitzenkörper (Spk), the apical cell surface, and developing septa. It was also present in numerous fine particles throughout the cytoplasm plus some large vacuoles in distal hyphal regions. Although the same general subcellular distribution was observed previously for CHS-3 and CHS-6, they did not fully colocalize. Dual labeling showed that the three different chitin synthases were contained in different vesicular compartments, suggesting the existence of a different subpopulation of chitosomes for each CHS. CHS-1–GFP persisted in the Spk during hyphal elongation but disappeared from the septum after its development was completed. Wide-field fluorescence microscopy and total internal reflection fluorescence microscopy revealed subapical clouds of particles, suggestive of chitosomes moving continuously toward the Spk. Benomyl had no effect on CHS-1–GFP localization, indicating that microtubules are not strictly required for CHS trafficking to the hyphal apex. Conversely, actin inhibitors caused severe mislocalization of CHS-1–GFP, indicating that actin plays a major role in the orderly traffic and localization of CHS-1 at the apex.

Chitin, a nonbranched homopolymer of β-1,4-*N*-acetylglucosamine (GlcNAc) residues, is widely found in the cell walls of yeasts and filamentous fungi, though its content and spatial distribution in the cell vary greatly among different species. Chitin content in filamentous fungi exceeds that in the yeast *Saccharomyces cerevisiae* (3, 7, 8, 33, 35). Chitin synthesis is catalyzed by chitin synthase (CHS; EC 2.4.1.16), an enzyme that transfers GlcNAc from UDP-GlcNAc to the nonreducing end of growing chitin chains (15). Cell fractionation analysis in *S. cerevisiae* revealed that CHS is present mainly in two locations: the plasma membrane and chitosomes (19). Extensive analysis of available fungal genome sequences revealed the presence of several genes that potentially encode chitin synthases (9, 22). Predicted peptide sequences suggest that CHSs are membrane-bound proteins with multiple transmembrane domains. Fungal CHSs have been grouped in three major divisions and seven different classes (30). Classes I, II, and III belong to CHS division 1 and contain a hydrophilic domain (Pfam 01644) in the N-terminal region of the catalytic domain. Classes IV, V, and VII are included in division 2, with classes IV and V containing the same catalytic domain (Pfam 03142), preceded by a cytochrome b_5-like domain (Pfam 00173). Only classes V and VII have a myosin motor head-like domain (MMD) (Pfam 00063) in the N-terminal region. Division 3, which includes only one class (class VI), has a conserved catalytic domain but none of the Pfam domains present in the other divisions. Classes III, V, VI, and VII are exclusively found in filamentous fungi (9, 22, 30). In *Neurospora crassa*, seven *chs* genes (*chs-1* to *chs-7*) have been found, each belonging to one of the seven different classes of CHSs (6, 14, 31).

The multiplicity of CHS genes and their corresponding proteins poses important questions as to their respective functions and indispensability. Recently, we reported that two CHS proteins of *N. crassa*, CHS-3 and CHS-6, tagged with green fluorescent protein (GFP), had similar intracellular distributions (31). These two proteins accumulated conspicuously in the core of the Spitzenkörper (Spk) of growing hyphal tips and in nascent septa but were also found in subapical regions in the form of spherical vacuoles, and—particularly CHS-6—in a network of irregular endomembranous compartments. Fluorescence recovery after photobleaching analysis suggested that CHS-GFP-containing microvesicles—i.e., chitosomes—are transported from subapical regions to the Spk and that these proteins utilize an alternative route to the classical secretory pathway (30, 31).

The mechanisms that control the localization and movement of cell wall-synthesizing enzymes in fungal hyphae are ultimately responsible for defining cell shape. Here we report the subcellular localization and requirements for transport of the *N. crassa* class III CHS (CHS-1) and compared them to those previously found for class I CHS-3 and class VI CHS-6.

* Corresponding author. Mailing address: Department of Microbiology, Center for Scientific Research and Higher Education of Ensenada (CICESE), P.O. Box 430222, San Ysidro, CA 92143-0222. Phone: (646) 175-0500, ext. 27051. Fax: (646) 175-0595, ext. 27052. E-mail: riquelme@cicese.mx.

† Supplemental material for this article may be found at http://ec.asm.org/.

▽ Published ahead of print on 4 February 2011.

TABLE 1. Plasmids, strains, and oligonucleotides used

Plasmid, strain, or oligonucleotide	Description, genotype, or sequence	Reference and/or source
Plasmids		
pMF272	P*ccg1*::*sgfp*$^+$	12
pMF357	P*ccg1*::*hH1*$^+$::*sgfp*$^+$::*hph*$^+$	This study
pESL01-1	P*ccg1*::*chs-1*::*sgfp*$^+$::5′Δ*his-3*	This study
pESL02-3	P*ccg1*::*chs-1*::*sgfp*$^+$::*hph*$^+$::3′ flank	This study
Strains		
N1	*mat a*	FGSC988
N150	*mat A*	FGSC2489
N39	*mat A*; *fl*	FGSC4317
N40	*mat a*; *fl*	FGSC4347
SMRP25	*mat a*; Δ*mus-51*::*bar*$^+$	FGSC9718
SMRP24	*mat A his-3*; Δ*mus-51*::*bar*$^+$	FGSC9717
NMR-3	*mat A his-3*$^+$::P*ccg-1*::*chs-3*::*sgfp*$^+$	31
NMR-6	*mat A his-3*$^+$::P*ccg-1*::*chs-6*::*sgfp*$^+$	31
NES2-11	*mat A*; *chs-1*::*sgfp*$^+$::*hph*$^+$	This study
SMRP52[a]	*mat a*; *chs-1*::*sgfp*$^+$::*hph*$^+$	This study
NES1-15	*mat A his-3*$^+$::P*ccg-1*::*chs-1*::*sgfp*$^+$	This study
SMRP53[a]	*mat A his-3*$^+$::P*ccg-1*::*chs-1*::*sgfp*$^+$	This study
NJV4.2.1	*mat A*; *gs-1*$^+$::*sgfp*$^+$::*hph*$^+$	39
NJV13.2	*mat A his-3*$^+$::P*ccg-1*::*chs-1*$^+$::*mchfp*$^+$; *gs-1*::*sgfp*$^+$::*hph*$^+$	39
TJV12-1[a]	*mat A*; *chs-1*::*mchfp*$^+$::*hph*$^+$	39
N2526	*rid*^{RIP1} *mat A his-3*$^+$::P*ccg-1*::*Bml*$^+$::*sgfp*$^+$	12; FGSC9520
SMRP18	*mat a*; Δ*chs-1*::*hph*$^+$	FGSC14318
SMRP66	*mat a*; Δ*chs-3*::*hph*$^+$	FGSC14320
SMRP58	*mat A*; Δ*chs-6*::*hph*$^+$	FGSC13408
Oligonucleotides[b]		
Chs1-XbaI-F-N	5′-GTCC**TCTAGA**ATGGCGTACCACGGTC-3′	This study
Chs1-PacI-R-N	5′-GCG**TTAATTAA**GCGACGGGCAAAGCA-3′	This study
Chs1-3′flank-F	5′-ACTG**GGTACC**CGCTAGGCAAACCCAAAACACG-3′	This study
Chs1-3′flank-R	5′-TACG**CTGCAG**AACCCGTCACGTCAGCAAAC-3′	This study
MRp10	5′-AGAGACAAGAAAATTACCCCCTTCTT-3′	31
MRp11	5′-AACTACAACAGCCACAACGTCTATATC-3′	31
MRp12	5′-ATAATGAACGGAAGGTAGTTGTAGAAAG-3′	31
MRp13	5′-ATGGATATAATGTGGCTGTTGAAAG-3′	31
pMF272F	5′-CAAATCAACACAACACTCAAACCA-3′	12
pMF272R2	5′-AGATGAACTTCAGGGTCAGCTTG-3′	31

[a] Heterokaryon.
[b] Bold type indicates restriction endonuclease sites.

MATERIALS AND METHODS

Strains and culture conditions. Bacterial and *Neurospora* strains used or generated in this study are listed in Table 1. *Escherichia coli* DH5α was grown on LB medium (1% tryptone, 0.5% yeast extract, 1% NaCl) supplemented with ampicillin (100 μg/ml) and incubated at 37°C. *Neurospora* cells were routinely grown on Vogel's minimal medium (VMM) with 1.5% sucrose and 1.5% agar if needed (41). For auxotrophic, His$^-$ strains, histidine (0.5 mg/ml) was added to VMM. Transformed conidia were plated on VMM-FGS (0.5% fructose, 0.5% glucose, 20% sorbose) medium that was supplemented with hygromycin B (200 μg/ml; Sigma) when required. For crosses, *mat a* conidia were spread over *mat A* mycelium grown on solid synthetic crossing medium with 2% sucrose (43). For growth analysis, elongation rates of *N. crassa* transformants and CHS mutant strains were measured on VMM agar plates at 30°C. Microscopy of all *N. crassa* strains was done at 22 to 24°C. CHS deletion mutants FGSC14318 (*mat a* Δ*chs-1*::*hph*$^+$), FGSC14319 (*mat A* Δ*chs-1*::*hph*$^+$), FGSC14320 (*mat a* Δ*chs-3*::*hph*$^+$), FGSC14321 (*mat A* Δ*chs-3*::*hph*$^+$), and FGSC13408 (*mat A* Δ*chs-6*::*hph*$^+$) were constructed as previously described (10) and obtained from the Fungal Genetics Stock Center (UMKC, Kansas City, MO).

Recombinant DNA techniques and plasmid constructions. Plasmids and oligonucleotides used are described in Table 1. Standard PCR and cloning procedures were used to fuse the *sgfp* gene to the carboxyl terminus of *chs-1* in plasmids pMF272 (12) and pMF357. The 2.8-kb open reading frame (ORF) of the *chs-1* gene (class III CHS; NCU03611.3) and a 0.97-kb fragment downstream of *chs-1* were identified in *N. crassa* (www.broad.mit.edu/annotation/genome/neurospora) and amplified by PCR from *N. crassa* N1 (FGSC988) genomic DNA with custom-designed primers that included XbaI/PacI and PstI/KpnI restriction endonuclease sites at their 5′ termini, respectively. PCR was performed in a Bio-Rad Thermal Cycler using Platinum *Taq* high-fidelity DNA polymerase (Invitrogen). For the *chs-1* gene, denaturation at 95°C (2 min) was followed by 25 to 30 cycles of 95°C (30 s), 58°C (30 s), and 72°C (6 min) and by a final extension at 72°C (5 min). For the *chs-1* 3′-flanking region, the conditions were similar, except that the annealing temperature was 61°C and the extension time was 70 s. The amplified and gel-purified *chs-1* PCR product was digested with XbaI and PacI and inserted into XbaI/PacI-digested pMF272 (12) (GenBank accession no. AY598428), yielding plasmid pESL01-1 (see Fig. S1A in the supplemental material). The amplified and gel-purified *chs-1* 3′-flanking PCR product was digested with KpnI and PstI and cloned into KpnI/PstI-digested plasmid pMF357. The resulting plasmid was XbaI/PacI digested to subclone the *chs-1* gene from pESL01-1 to generate pESL02-3 (see Fig. S1B in the supplemental material). All plasmids were propagated in *E. coli* DH5α and purified with QIAprep Spin Miniprep kits (Qiagen). Plasmid inserts were sequenced at the Core Instrumentation Facility of the Institute for Integrative Genome Biology at the University of California, Riverside, CA, with primers pMF272F and pMF272R2.

***Neurospora* genetics.** Conidia of *N. crassa* host strains FGSC9717 and FGSC9718, which are both deficient in the nonhomologous end-joining process (27), were transformed with linearized plasmids pESL01-1 (NdeI digested) and pESL02-3 (SspI digested), respectively, by electroporation in a Bio-Rad Gene Pulser (capacitance, 25 μF; voltage, 1.5 kV; resistance, 600 Ω) as previously

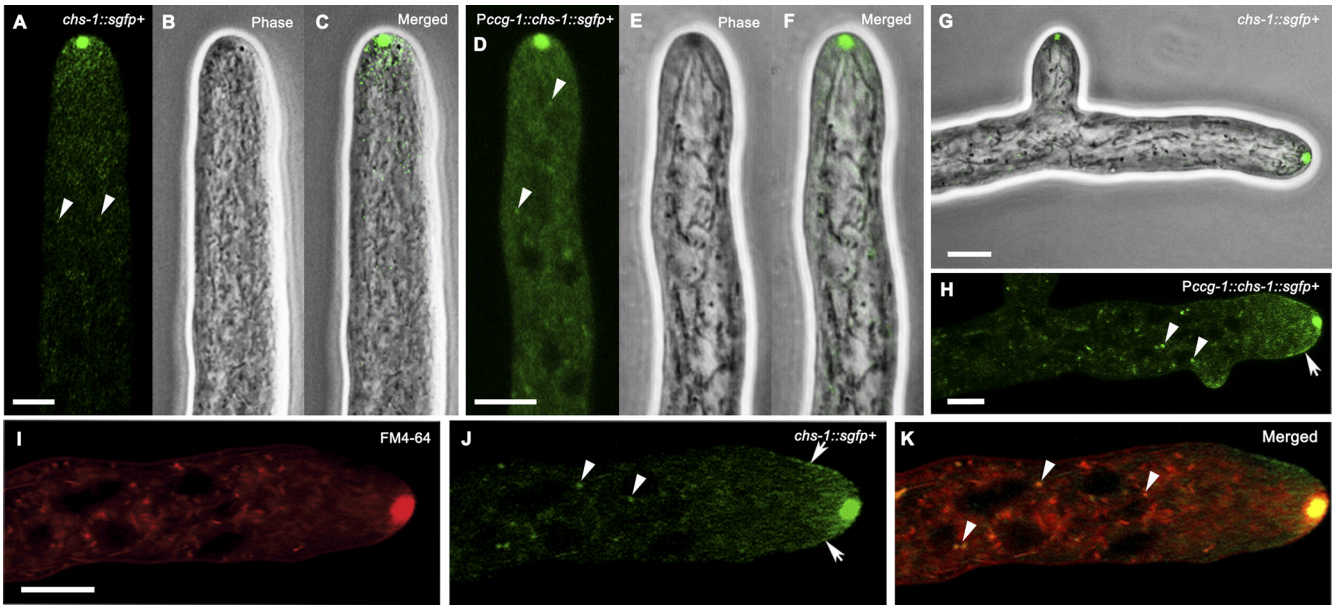

FIG. 1. LSCM analysis of the distribution of CHS-1–GFP in the growing apices of *Neurospora crassa* hyphae. All hyphae show one intense fluorescent spot coinciding with the Spk core and punctate fluorescence in the subapical regions (A to K). Comparison of *N. crassa* strains NES1-15 (P*ccg-1*::*chs-1*::*sgfp*$^+$) and NES2-11 (*chs-1*::*sgfp*$^+$) showed no apparent differences between CHS-1–GFP expressed under the control of the native *chs-1* gene promoter (A, C, G, and J) and that expressed under the control of the *ccg-1* promoter (D, F, and H). The Spk core area occupied by CHS-1–GFP in all growing hyphae coincided with the phase-dark Spk observed in leading hyphae (C and F). Panels H and J show evidence of accumulation of fluorescence at the cell surface of the apical and subapical regions (white arrows). Panels I to K show comparison of the localizations of CHS-1–GFP with the lipophilic dye FM4-64. Note mostly the lack of coincidence with only partial overlap at the core of the Spk and at some subapical vesicles (arrowheads). Bars, 5 μm.

described (31). For each transformation, 20 to 30 histidine prototrophs (His$^+$) or hygromycin B (200 μg/ml)-resistant (Hyg$^+$) transformants were transferred to VMM slants and screened for the expression of CHS-GFP by epifluorescence microscopy under an inverted microscope (Zeiss Axiovert 200). Transformants TES2-11 (*mat a chs-1*::*sgfp*$^+$::*hph*$^+$) and TES1-15 (*mat A his-3*$^+$::P*ccg-1*::*chs-1*::*sgfp*$^+$), which showed the highest fluorescence, were crossed to strains N150 (FGSC2489; *mat A*) and N1 (FGSC988; *mat a*), respectively. Random ascospores were heat shocked on VMM at 60°C for 1 h and transferred to 25°C to obtain homokaryons. After analysis of the resulting germinated ascospores, two strains were selected for further analysis, NES2-11 and NES1-15. Mating type was determined by spot testing on *fluffy* strains N39 (FGSC4317; *mat A fl*) and N40 (FGSC4347; *mat a fl*) (Table 1).

To evaluate the insertion of *chs-1*::*sgfp*$^+$ at the *his-3* locus of TES1-15 (*mat a chs-1*::*sgfp*$^+$::*hph*$^+$), PCR of genomic DNA with primers MRp10 and MRp11 or MRp12 and MRp13 (Table 1) was performed. For confirmatory Southern blot analyses, genomic DNA from strains SMRP24, SMRP25, NES2-11, and NES1-15 was obtained as previously described (31), digested with BamHI, separated on a 0.7% agarose gel, blotted to charged nylon membranes, and probed with a digoxigenin (DIG)-labeled *chs-1* fragment generated with a nonradioactive labeling kit (DIG High Prime DNA labeling and detection starter kit II; Roche Applied Science) (see Fig. S2 in the supplemental material).

Microscopy and image processing. Hyphal morphology at the colony edges was imaged with a stereoscopic microscope (Olympus SZX12) coupled to a high-resolution Olympus DP70 digital camera. Elongation rates of mutant strains were measured with the DP Controller 1.1.1.65 software (2002 Olympus Optical Co., Ltd.). Wide-field fluorescence images of the transformants were obtained with an inverted microscope (Zeiss Axiovert 200) fitted with a GFP filter and coupled to a high-resolution digital camera (Zeiss Axiocam HRc). A 100× Ph3 Plan Neofluar oil-immersion objective (numerical aperture [NA], 1.3) was used for image acquisition, and the images were captured with AxioVision LE release 4.5 software (Carl Zeiss). For confocal microscopy, growing hyphae were imaged at 22 to 24°C with an inverted Zeiss LSM-510 Meta laser scanning confocal microscope (LSCM) fitted with an argon/2 ion laser (GFP: excitation, 488 nm; emission, 515 to 530 nm). For simultaneous visualization of GFP and mCherry expression, an argon/2 and He/Ne-2 ion laser was used (red/mCherry: excitation 543 nm; emission, 585 to 615 nm). A 100× Ph3 Plan Neofluar oil-immersion objective (NA, 1.3) was used for all confocal observations. Confocal images were captured using LSM-510 software (version 3.2; Carl Zeiss), evaluated with an LSM-510 image examiner (version 3.2), and further processed with Adobe Photoshop CS2 (version 10.0). Selected image series were converted into movies with the same software. For time-lapse and live-cell imaging, the "inverted agar block method" was employed (17). To analyze the *in vivo* colocalization of CHS-1 with microtubules (MTs), other CHS proteins, and glucan synthase-related protein (GS-1), we generated hyphal fusions on VMM agar plates, where two different *N. crassa* strains of the same mating type were inoculated side by side and grown overnight at 30°C. For epifluorescence microscopy, we used an inverted Olympus 1X81 microscope with a motorized focus module, equipped with a 40× water-immersion objective, and a mercury-xenon lamp (150 W) connected by quartz optic fibers. Images were acquired with a Hamamatsu charge-coupled device (CCD) Orca-ER C4742-80 digital electron multiplication (EM) monochromatic camera. For total internal reflection fluorescence microscopy (TIRFM), an IX-70 inverted microscope equipped with a 60×/1.45 Apochromat objective lens (Olympus America Inc., Center Valley, PA) and a krypton/argon laser (Melles Griot, Carlsbad, CA) (488 nm) was used. Images were recorded with a Cascade 512B EM-CCD camera (Photometrics, Tucson, AZ) for durations of 2 to 3 min at 512-by-512 resolution and rates of 10 frames/s. MetaMorph 6.1 software (Universal Imaging, Downingtown, PA) was used to control the camera and capture images. MetaMorph 7.5.0 was used to analyze and process TIRFM time series and to obtain kymographs. Kymographs describe motion patterns of fluorescent particles in specific regions during cell growth. This type of analysis allowed us to depict velocity variations of individual vesicles during their intracellular traffic. The *x* and *y* axes of the kymographs represent the particle moving distance analyzed during a specific time, respectively. Regions analyzed were obtained by setting areas of interest in the time series, which allowed tracking of the vesicle dynamics in a continuous mode.

Fluorescent dyes and inhibitors. Two organelle-specific dyes were used in this study. For staining of vacuolar content, we used the cell-permeable esterase diacetate derivative of carboxydifluorofluorescein (CCDFDA; Oregon Green; Invitrogen/Molecular Probes; 10 μM). For staining of endocytic organelles, we used the styryl dye *N*-(3-triethylammoniumpropyl)-4-(6-[4-{diethylamino}phenyl] hexatrienyl)pyridinium dibromide (FM4-64; Molecular Probes; 25 μM). A stock solution (500 μg/ml) of the antimicrotubule agent methyl 1-(butylcarbamoyl)-2-benzimidazolecarbamate (benomyl; Sigma) was prepared in ethanol and diluted in VMM to a working concentration of 10 μg/ml.

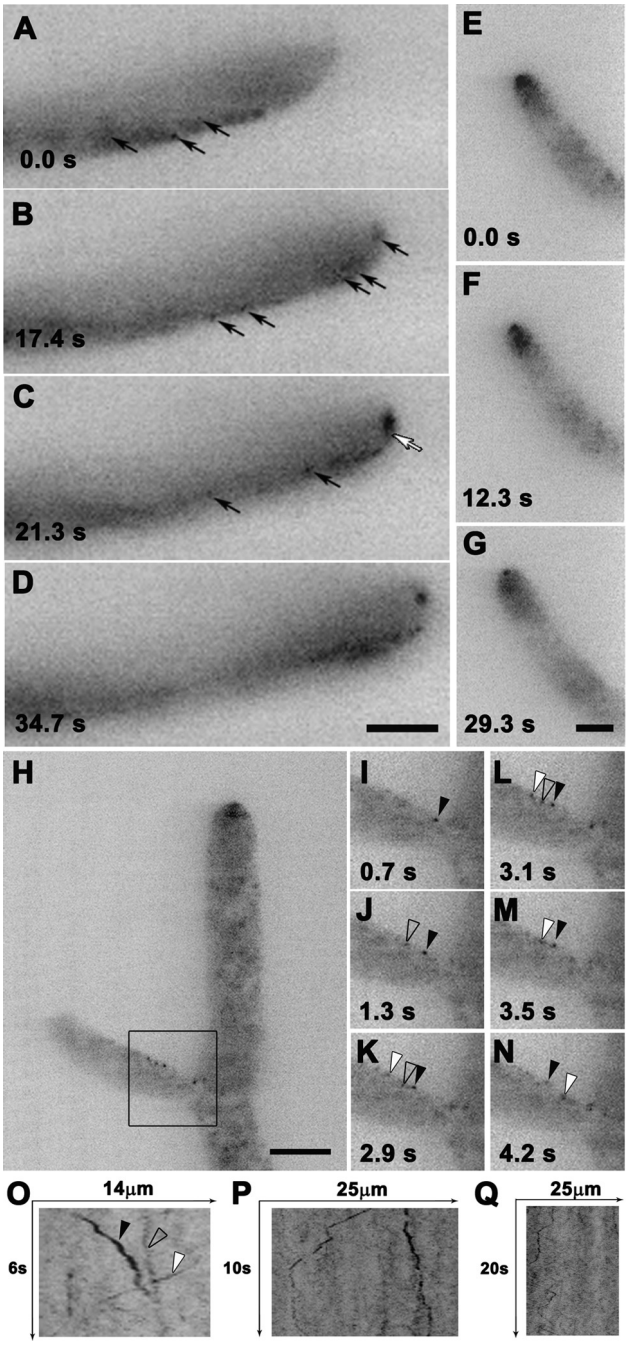

FIG. 2. Analysis of CHS-1–GFP vesicle movement by total internal reflection microscopy in *N. crassa* NES2-11. Time series showing anterograde advancement of a group of vesicles (A to D) (black arrows) at the periphery of the cell toward the Spk (C) (white arrow). Bar, 5 μm. Frames from a time series (see Movie S4 in the supplemental material) showing a dense subapical cloud of vesicles reaching the Spk (E to G). Bar, 5 μm. Individual vesicles observed moving in a lateral branch (I to N). Bar, 10 μm. Frames corresponding to the box in panel H showing the forward advancement of a vesicle (solid black arrowheads), the retrograde movement of another vesicle (solid white arrowheads), and a vesicle that does not move (empty arrowheads) (I to N). Graphical representation of spatial position over time (kymograph) of CHS-1–GFP vesicles in panels I to N (O). Vertical lines represent stationary signals. Kymographs showing the moving patterns of different vesicles in regions near the tip of leading hyphae from other recorded sequences not shown (P and Q).

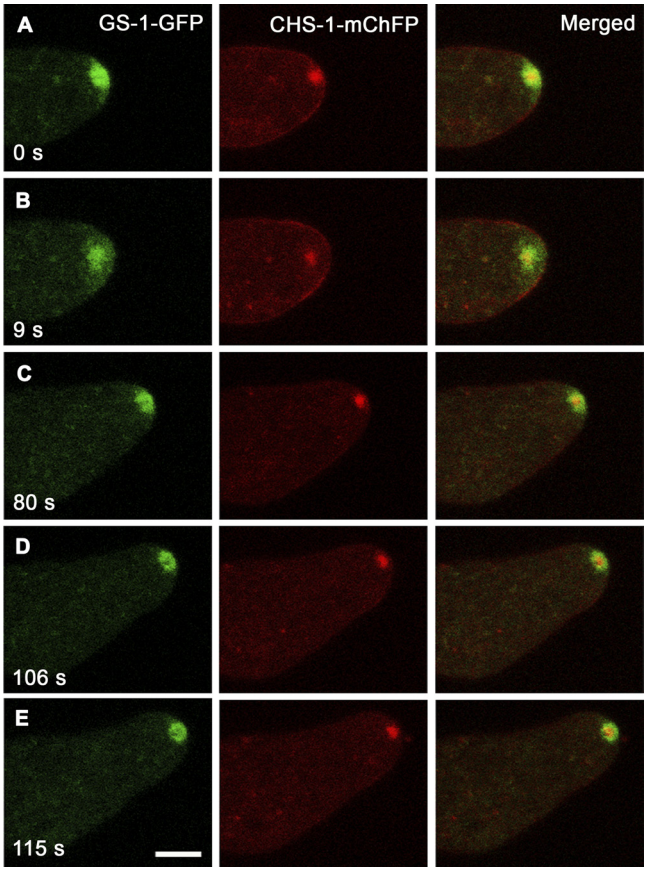

FIG. 3. Differential localizations of CHS-1–mChFP and GS-1–GFP in an *N. crassa* strain expressing both fusion proteins. In the Spk, there is clear stratification with the CHS-1–mChFP in the center and the GS-1–GFP toward the outside (Spitzenring). The GS-1–GFP-labeled layer sometimes adopted a horseshoe-like form whose opening faced different directions (left column), whereas the CHS-1–mChFP-labeled Spk core remained largely similar in morphology (center column). Note in panel B a momentary simultaneous retraction of the Spk core and the Spitzenring. During that event, the CHS-1–mChFP signal at the apical cell surface became more evident. Bar, 5 μm.

Cytochalasin A (CA; Sigma) stock solution (10 mg/ml) was prepared in dimethyl sulfoxide and used at a final concentration of 10 μg/ml in VMM. Latrunculin A (LatA; Sigma) stock solution (1 mM) was prepared in dimethyl sulfoxide and used at a final concentration of 20 μg/ml in VMM. A stock solution (20 mg/ml) of the fungal metabolite brefeldin A (BFA; Sigma) was prepared in dimethyl sulfoxide and used at a final concentration of 5 μg/ml in VMM. For each dye or inhibitor, the agar blocks with hyphae were inverted onto coverslips with 5- to 10-μl drops of the diluted working stock. Stained or treated cells were imaged 3 to 5 min after recovery.

RESULTS

In mature hyphae, CHS-1–GFP localizes predominantly in the Spk core region. In all growing hyphae examined, CHS-1–GFP was conspicuously found in the core of the Spk; this was true for both leading hyphae and lateral branches (Fig. 1; see Fig. S3 and Movie S1 in the supplemental material). The fluorescence of CHS-1–GFP coincided with the position of the phase-dark Spk. The membranous marker FM4-64 stained a larger Spk area than that outlined by CHS-1–GFP; the latter was mainly restricted to the central or "core" region of the Spk

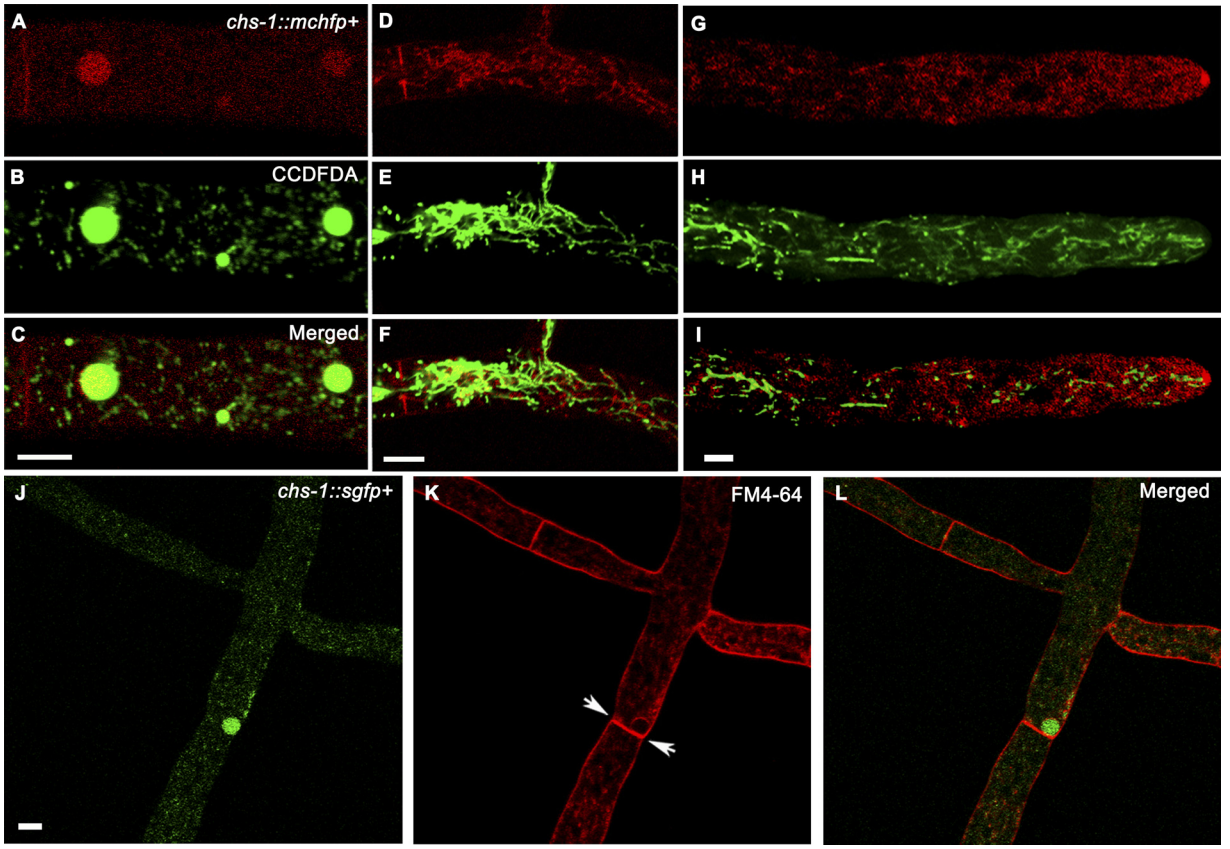

FIG. 4. Localization of CHS-1 at vacuoles in distal hyphal regions. CCDFDA and FM4-64 fluorochromes were used to stain the vacuolar network and endomembrane network, respectively, in both *N. crassa* strains TJV12-1 (CHS-1–mChFP) and TES1-15 (CHS-1–GFP). CCDFDA stained an intricate network of tubular vacuoles in the subapical and distal regions of the hyphae (B, E, and H). Label intensity increased toward the distal areas. The only CHS-1–mChFP-labeled structures that colocalized with the vacuolar marker were some large globular vacuoles (B and C). FM4-64 staining revealed CHS-1–GFP localization in the lumen of the globular vacuoles (J to L). Note the absence of CHS-1–GFP at a fully developed septum stained with FM4-64 (arrows in panel K). Bars, 5 μm.

(n = 19) (Fig. 1I to K). As the hypha elongated, the Spk with its CHS-1–GFP-containing core moved forward, accompanied by characteristic minor lateral movements and pleomorphic changes (see Movie S1 in the supplemental material). There was also accumulation of CHS-1–GFP at the cell surface in the apical and subapical hyphal regions (arrows in Fig. 1H and J). Small fluorescent particles were found scattered over the entire length of the hyphae examined (Fig. 1A, D, H, and J). Since in several other studies in *Neurospora* the expression of GFP constructs has been driven by the *ccg-1* promoter, we determined if expression of CHS-1–GFP was affected by different promoters, specifically whether *his-3*-targeted CHS-1–GFP from the *ccg-1* promoter significantly changed localization patterns compared to expression of CHS-1–GFP at the endogenous locus. LSCM analysis of NES1-15 (P*ccg-1*::*chs-1*::*sgfp*$^+$) and NES2-11 (*chs-1*::*sgfp*$^+$) in both cases ($n \geq 30$) revealed no significant differences in CHS-1–GFP localization (Fig. 1). The only noticeable difference was that under the native promoter, less background fluorescence was observed and therefore that strain was the one selected for further analyses.

Wide-field epifluorescence microscopy showed a high concentration of CHS-1–GFP directly behind the Spk (see Movies S1 and S2 in the supplemental material). This mass of small, rapidly moving fluorescent particles appeared to merge with the Spk core. With the finer detail and better temporal resolution of TIRFM, we could observe the movement of this mass of particles reaching the Spk (Fig. 2E and F; also see Movie S4 in the supplemental material). Some of the fluorescent particles evidenced by TIRFM seemed to move along the hyphal periphery (Fig. 2H to N; see also Movie S3). However, by changing the angle of incidence of the laser, we were able to observe beneath the cell periphery and could image the particles (vesicles) moving in the interior of the hypha (Fig. 2A to G). Most vesicles moved in an anterograde fashion, although some moved in a retrograde manner (Fig. 2H to N). Analysis of the dynamics of three fluorescent vesicles in a lateral branch showed one vesicle moving fast toward the tip and the other two moving in a retrograde manner but at different speeds (Fig. 2O). Kymograph analysis in different hyphae revealed different motion patterns of vesicles (Fig. 2P and Q). The speeds of anterograde and retrograde moving vesicles were on average 3.8 ± 0.9 and 3.6 ± 0.9 μm/s, respectively (n = 20 for each).

Spatial relationship between vesicular populations involved in glucan and chitin synthesis. Previously, we found that GS-1, a glucan synthase-related protein, was localized in a subpopu-

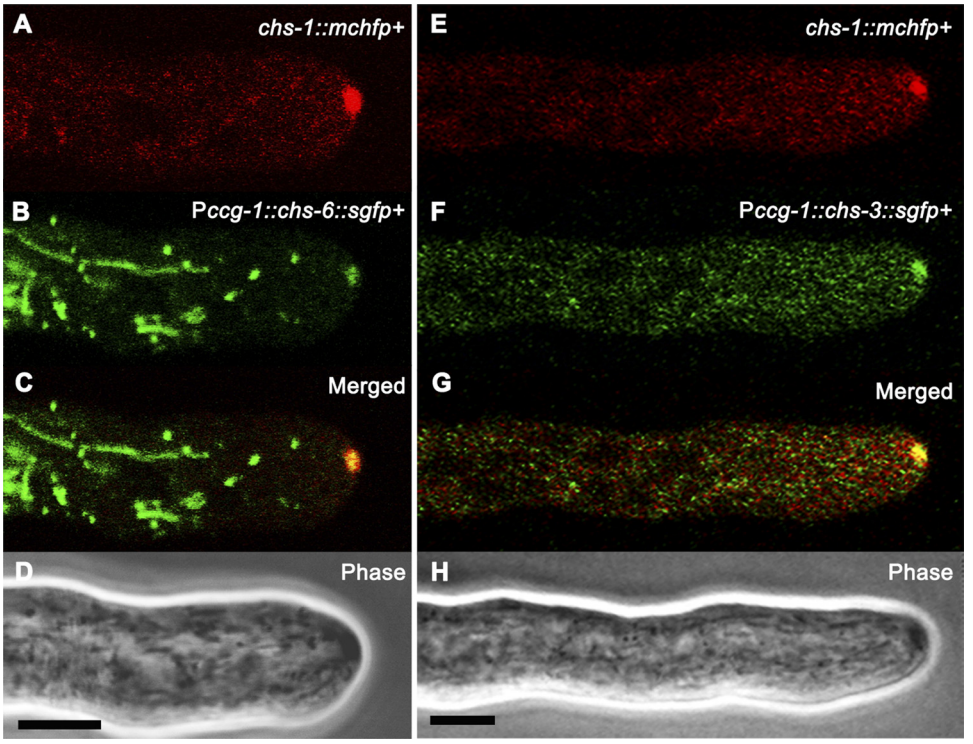

FIG. 5. Differential localizations of CHS-1, CHS-3, and CHS-6 in *N. crassa* hyphae. LSCM analysis of a hypha coexpressing CHS-1–mChFP and CHS-6–GFP showed distinctly different localizations of these markers (A to D). In the Spk, the GFP fluorescence of CHS-6 was restricted to a smaller area than that of mChFP fluorescence of CHS-1. In the subapical regions of the hypha, intense CHS-6–GFP fluorescence was observed in a tubular vacuolar network, whereas CHS-1–mChFP localized mainly in punctate structures. Similar comparison of CHS-1–mChFP and CHS-3–GFP showed near-coincidence in Spk localization (E to H). However, in the subapex and distal regions of the hypha the merged image (G) shows two different vesicle populations: vesicles with red fluorescence (CHS-1–mChFP) were clearly separated from green fluorescent vesicles (CHS-3–GFP). Bars, 5 μm.

lation of vesicles that accumulated in the outer stratum of the Spk (39). To further analyze the dynamic relationship between the different Spk components, strains NJV4.2.1 (GS-1–GFP) and TJV12-1 (CHS-1–mChFP) were vegetatively fused and examined by confocal laser scanning microscopy (Fig. 3). CHS-1–mChFP appeared as a solid round apical body surrounded by a layer of GS-1–GFP. Overall, the intensity, position, and behavior of CHS-1–mChFP (Spk core) remained relatively constant as the hypha advanced, although with the typical minor oscillations of a Spk. In contrast, the structure highlighted by GS-1–GFP (Spitzenring) was more dynamic, adopting horseshoe-like forms with the opening facing different directions as the hypha grew (Fig. 3; see also Movie S5 in the supplemental material), thus suggesting that it rotated around the microvesicular core. A sudden retraction of the Spk showed both the core and the Spitzenring behaving as a unit (Fig. 3B). Once the Spk regained its position at the center of the apical dome, the hypha continued to grow, although it initially had a more pointed appearance and a reduced diameter.

In distal regions of mature hyphae, CHS-1 is localized in the tubular vacuolar network. The vacuolar dye CCDFDA was used to analyze the nature of the compartments harboring CHS-1–mChFP or CHS-1–GFP fluorescence. CCDFDA staining in the *Neurospora* strain TJV12-1 revealed a very dynamic and extensive tubular and spherical vacuolar network along the hyphae (Fig. 4B, E, and H), in both distal and subapical regions. CHS-1–GFP or CHS-1–mChFP was observed within globular vacuoles as well but only in distal regions of hyphae (Fig. 4A and J). The FM4-64 lyophilic probe stained the membrane of globular vacuoles, confirming that fluorescently labeled CHS-1 occupied the lumen of these presumed vacuolar structures (Fig. 4J to L).

Coimaging of CHS reveals differential localization of CHS-1, CHS-3, and CHS-6. To analyze whether CHS-1–GFP was an integral part of the same subcellular compartments where CHS-3–GFP and CHS-6–GFP were found to be present (31), we generated heterokaryons by hyphal fusion between each one of these strains and strain TJV12-1 (expressing CHS-1–mChFP). Although we found that CHS-1–mChFP and CHS-6–GFP were located in the Spk, the fluorescence of CHS-1–mChFP occupied a larger area than that of CHS-6–GFP fluorescence (Fig. 5A to C). Also, CHS-1–mChFP did not label the numerous globular and tubular structures labeled by CHS-6–GFP in the subapical regions of the hyphae (Fig. 5B and C). Although we found no distinction between CHS-1–mChFP and CHS-3–GFP in the Spk, where both occupy the same area of the Spk core (Fig. 5E to G), in the apical and subapical cytoplasm, two distinctly separate subpopulations of vesicles were clearly evident (Fig. 5G).

CHS-1–GFP localization in developing septa. A strong fluorescent band of CHS-1–GFP was observed in all developing septa (Fig. 6; see Fig. S3 in the supplemental material). In

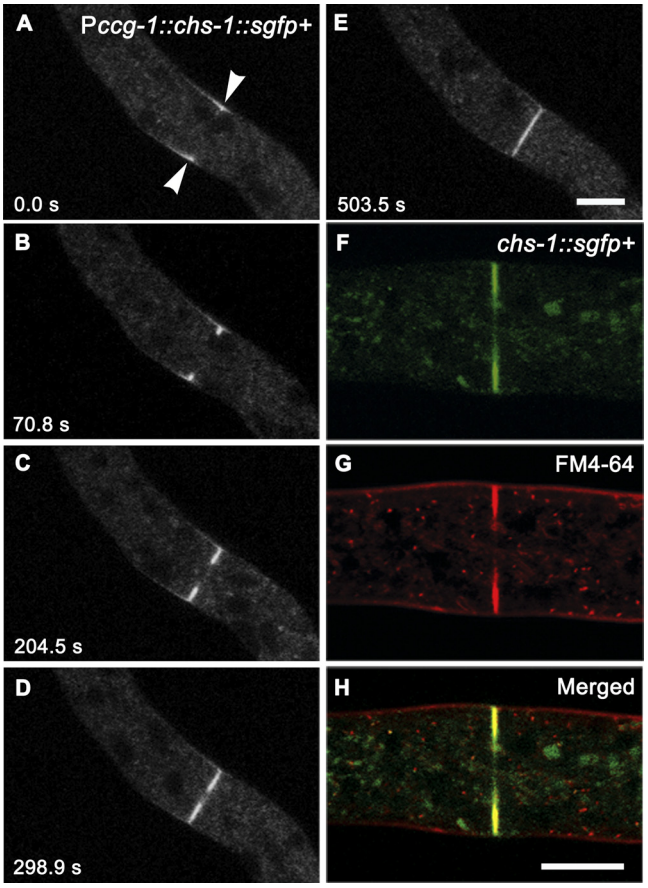

FIG. 6. CHS-1–GFP accumulation in developing septa. A sleeve of CHS-1–GFP accumulated in cortical areas of the hypha prior to septum formation (A) (arrowheads). A fluorescent ring can be seen growing centripetally until a full septum is formed (B to E). FM4-64 staining revealed the colocalization with CHS-1–GFP in a developing septum (F to H). Bars, 5 μm.

two-dimensional optical sections, the first indication of impending septation was a growing accumulation of CHS-1–GFP that appeared as symmetrical thickening of the hyphal wall (Fig. 6A). In three dimensions (3-D), this corresponds to a cylindrical "sleeve" of CHS-1–GFP. As this sleeve shortened, a fluorescent ring began to grow inwardly from the middle of the sleeve, with the typical morphology of a fungal septum (Fig. 6B and C; see also Movie S6 in the supplemental material). The fluorescent septum grew inward and narrowed the opening until it reached the size of a typical septal pore of *N. crassa* (Fig. 6D; see also Movies S6 and S7 in the supplemental material). This process lasted on average 6 min ($n = 5$). Gradually, over the course of approximately 1 h, the entire CHS-1–GFP fluorescence of the septal ring faded until the GFP signal was no longer detectable. Staining with FM4-64 showed colocalization of CHS-1–GFP with the invaginating plasma membrane during septum development ($n = 10$) (Fig. 6F to H). FM4-64 fluorescence persisted at the septum even after GFP fluorescence vanished (Fig. 4J to L).

CHS-GFP localization in germinating conidia. During germ tube emergence, there was no conspicuous accumulation of CHS-1–GFP, CHS-3–GFP, or CHS-6–GFP at the sites of polarized growth (Fig. 7). Young germlings (<100 μm in length or grown for less than 9 h) of *N. crassa* expressing CHS-1–GFP and CHS-3–GFP showed discrete fluorescent patches of different sizes, scattered through the germ tube (Fig. 7A and D) and not visible in the corresponding strain used for the transformations (Fig. 7J). In some of the germlings, a diffuse phase-dark cloud was observed by phase-contrast microscopy at the apical region (Fig. 7E and H). Yet, at this stage no distinct Spk could be observed.

The actin cytoskeleton is required for CHS-1–GFP localization at the Spk and the septum. Inhibitor studies were undertaken to examine whether MTs or actin was involved in CHS-1 transport. To study the effect of benomyl, we first generated dually labeled heterokaryons of strains TJV12-1 (CHS-1–mChFP) and N2526 (tubulin-GFP) to image GFP-labeled tubulin and mChFP-labeled CHS-1 simultaneously. In heterokaryotic hyphae, GFP clearly labeled the expected large number of cytoplasmic MTs (12, 25), while mChFP labeled the Spk core with intense red fluorescence (Fig. 8A and F). Within 4 min after benomyl was applied to the heterokaryon, all MTs had become depolymerized, leaving only small fluorescent particles corresponding to tubulin subunits (arrows in Fig. 8B). During the first 20 to 25 min after benomyl treatment, hyphae showed highly distorted morphology and decreased growth (Fig. 8C), as previously reported (25). During this period of strong growth impairment, no Spk could be observed in the distorted hyphae and therefore there was no accumulation of CHS-1–mChFP at the apex (Fig. 8C). However, 5 to 10 min later, when still no repolymerized GFP-labeled MTs were visible, hyphae started to recover and grow, and CHS-1–mChFP continued to accumulate at the Spk of distortedly and slow-growing hyphae (Fig. 8D and E). Once the cells recovered from the treatment (grew out of the inhibitory zone) and reached high growth rates, MTs gradually became visible again, concomitantly with the reestablishment of normal hyphoid morphology (Fig. 8F). CHS-1–mChFP accumulation at septa was also unaffected by the benomyl treatment (Fig. 8G).

In contrast to the results with benomyl, CA and LatA, which bind to F-actin and G-actin, respectively, therefore preventing actin microfilament assembly, affected CHS-1 localization drastically. LSCM observations of hyphae treated with 10 μg/ml CA revealed gross mislocalization of CHS-1–GFP (Fig. 8H to N). In apical regions, fluorescence was observed distributed in large patches that grew inwardly, developing one or multiple concave structures (Fig. 8H to L; see also Movie S8 in the supplemental material). At the septa, fluorescence accumulated unevenly, probably representing abortive nascent septa (Fig. 8M). One of the overall effects of CA was the previously described dichotomous apical branching giving the appearance of a candelabrum (Fig. 8N) (32). LatA-treated hyphae showed also cortical accumulations of CHS-1–GFP at subapical areas (Fig. 8P to S). Immediately after addition of LatA, the hyphal tips swelled and a Spk was no longer observable (Fig. 8O). As observed for CA, in LatA-treated cells, fluorescence accumulated unevenly at septa (Fig. 8T and U). Another intriguing effect of LatA was the accumulation of fluorescence at the membrane of globular vacuoles (Fig. 8T), instead of the typical accumulation at the vacuolar lumen.

CHS-1 reaches the Spk unaffected by brefeldin A. To evaluate if CHS-1–GFP follows the conventional secretory path-

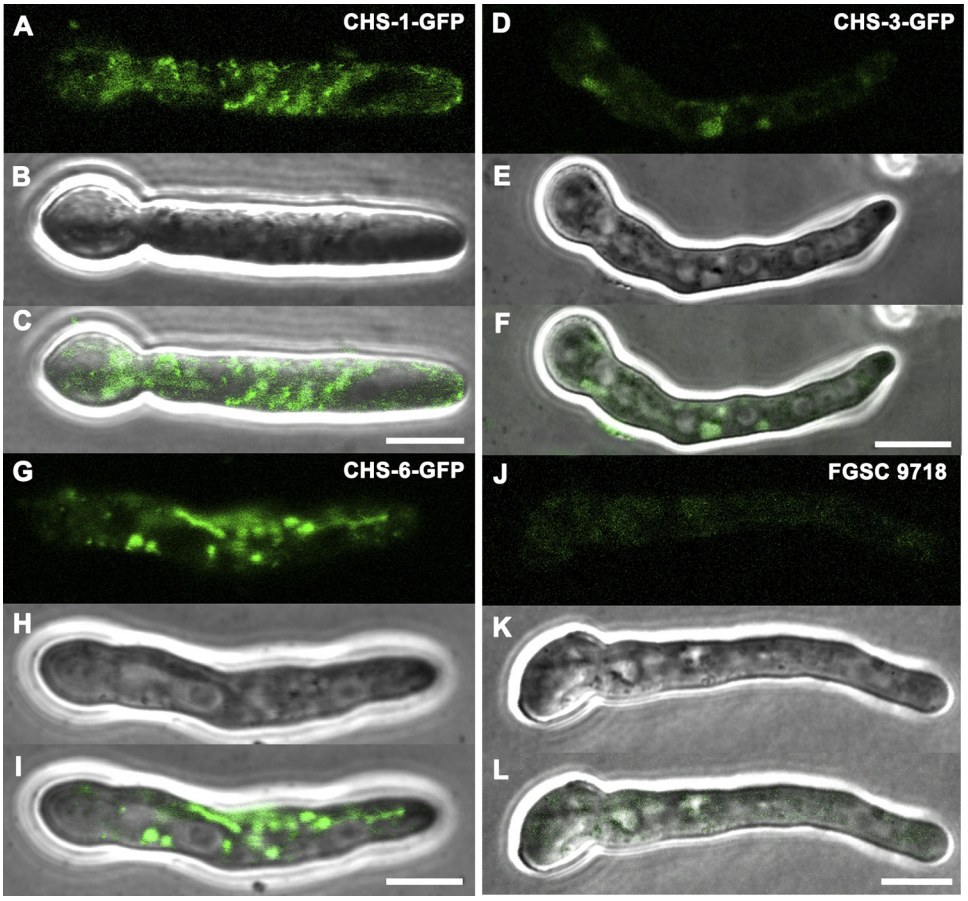

FIG. 7. Localizations of CHS-1, CHS-3, and CHS-6 tagged with GFP during early germ tube development. CHS-1–GFP and CHS-3–GFP fluorescence was randomly distributed along the germlings (A and D, respectively), whereas CHS-6–GFP fluorescence accumulated at small globular and tubular vacuoles (G). No fluorescence could be observed accumulating at the apical region of germ tubes expressing any of the fusion proteins (A, D, G, and J). No fluorescence was observed in germlings of *N. crassa* strain FGSC9718, the parental strain used for transformations. Bars, 5 μm.

way, we used brefeldin A (BFA), an inhibitor of endoplasmic reticulum (ER)-to-Golgi complex traffic, on strain NES2-11. BFA reduced the hyphal elongation rate drastically in a dose-dependent manner (Fig. 9A). LCSM revealed that the distribution of CHS-1–GFP was not altered in treated hyphae (Fig. 9). More interestingly, we found a slight increase in CHS-1–GFP accumulation at the Spk and apical plasma membrane in some hyphae (Fig. 9B and C). In addition, colonies exposed to BFA showed an increase in branching (Fig. 9D and E).

Effect of *chs* deletions on hyphal phenotype. Southern blotting and PCR analyses of selected strains confirmed the expected genotypes (see Fig. S2 in the supplemental material). The absence of *chs-1* in the Δ*chs-1* strain was confirmed by PCR (see Fig. S2F in the supplemental material). Growth, colony, and hyphal morphology were examined in three deletion mutants (Δ*chs-1*, Δ*chs-3*, and Δ*chs-6* strains) and compared to the CHS-1–GFP and the corresponding host strains used for transformation (Fig. 10). Elongation rates of both P*ccg-1*::*chs-1*::*sgfp*$^+$ or *chs-1*::*sgfp*$^+$ strains and their corresponding host strains were comparable to those obtained with *Neurospora* P*ccg-1*::*chs-3*::*sgfp*$^+$, P*ccg-1*::*chs-6*::*sgfp*$^+$, and wild-type strains, reported earlier (29, 31). Elongation rates of the *chs-1*::*sgfp*$^+$ (39.2 ± 3.9 μm/min, $n = 3$) and P*ccg-1*::*chs-1*::*sgfp*$^+$ (36.9 ± 4.4 μm/min, $n = 8$) transformants were not significantly different from those of the Δ*mus-51*::*bar*$^+$ (46.2 ± 3.0 μm/min, $n = 6$) and *his-3*; Δ*mus-51*::*bar*$^+$ (39.2 ± 5.9 μm/min, $n = 6$) parental strains, respectively. Growth of Δ*chs-1* and Δ*chs-3* strains (37.0 ± 1.1 μm/min, $n = 3$, and 35.2 ± 2.2 μm/min, $n = 3$, respectively) showed a slight growth rate reduction compared to that of the Δ*mus-51*::*bar*$^+$ strain. Growth of the Δ*chs-6* strain (23.2 ± 4.4 μm/min, $n = 3$) was significantly reduced (Fig. 10N). Observations of the colony margins revealed no gross differences between host strains used for transformations, *chs-1*::*sgfp*$^+$-expressing strains, and the Δ*chs-1* strain (Fig. 10). Hyphal diameters and overall branching patterns were similar in all strains.

DISCUSSION

Different populations of chitosomes. In addition to showing that CHS-1 is distributed in the hyphae of *N. crassa* mainly in the same locations previously reported for CHS-3–GFP and CHS-6–GFP (31), namely, the sites of new cell wall synthesis (growing apices and developing septa) plus numerous particles of various sizes distributed along the cyto-

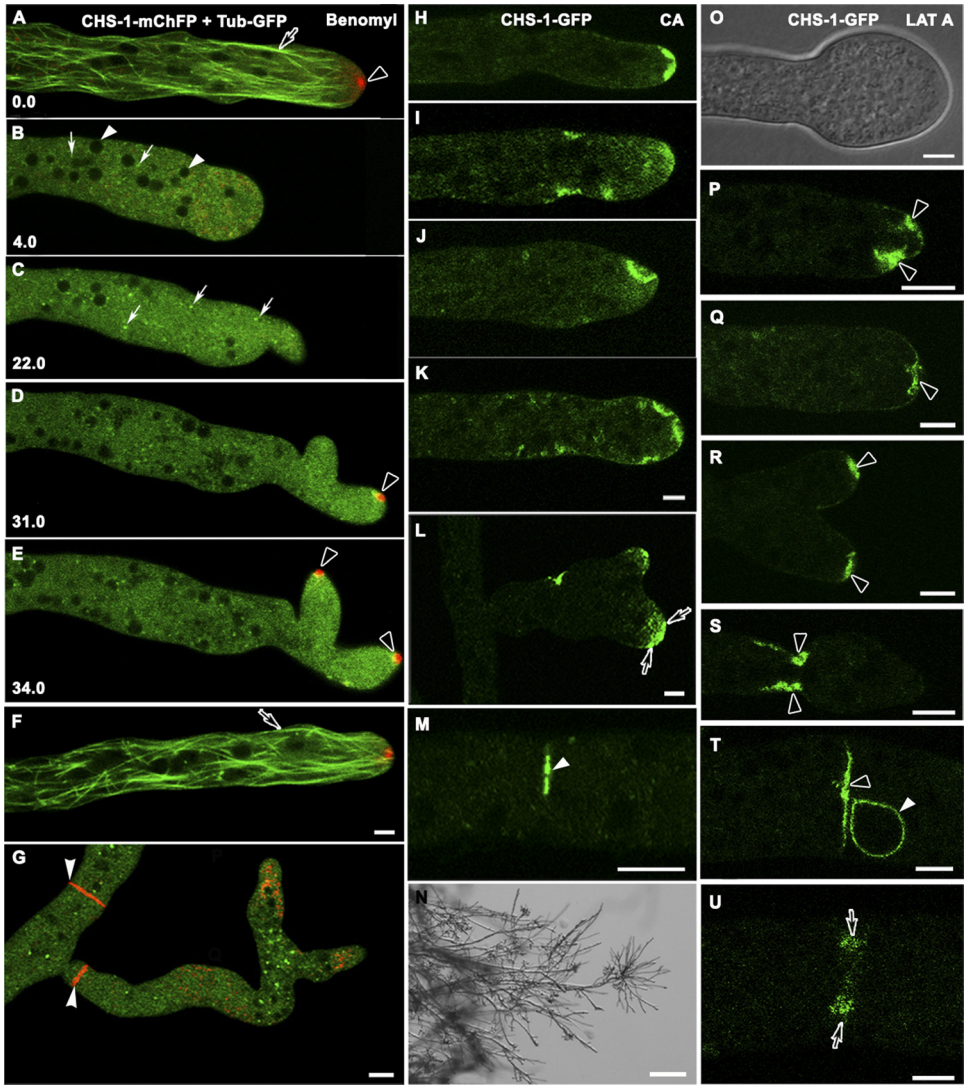

FIG. 8. Effect of cytoskeletal inhibitors on CHS-1–GFP localization. Microtubule inhibition (A to G). LSCM analysis of *N. crassa* hyphae coexpressing CHS-1–mChFP and tubulin-GFP treated with 10 μg/ml of benomyl. Untreated hyphae showing CHS-1–mChFP in the Spk (A) (arrowhead) and a great abundance of long GFP-labeled microtubules along the hypha (arrow) that seem to reach the apical dome. Microtubules are quickly and completely depolymerized, and small fluorescent patches—tubulin subunits—appear (B) (white arrows); nuclei change from pear shaped to round (B) (white arrowheads); the hypha loses its hyphoid shape and grows more isotropically. During that time, no Spk could be observed (B and C), but when polarized growth was resumed (D and E), CHS-1–mChFP fluorescence reappeared at the growing tips, even though microtubules remained depolymerized. When the inhibitory effect had disappeared, repolymerization of MTs could be observed (F). CHS-1–mChFP localization at the septal ring was unaffected by benomyl (G) (white arrowheads). Actin inhibition (H to N). Treatment of the CHS-1–GFP-expressing strain NES2-11 with 10 μg/ml cytochalasin A (CA) disrupted hyphal growth and modified the distribution of fluorescence in apical and subapical regions. CHS-1–GFP no longer accumulated at the Spk; instead, several fluorescent crescent-shaped structures were observed in the apical and subapical regions immediately under the cell surface (H to L). Deposition of CHS-1–GFP at nascent septa was disrupted under the effect of CA (M) (white arrowhead). A typical dichotomous branching (candelabrum) pattern at the edge of colonies exposed to CA was observed by phase-contrast microscopy (N). Effects of 20 μg/ml latrunculin A (LatA) on NES2-11 (O to U). Initial swelling of hyphal tips as result of the drug exposure observed by phase-contrast microscopy (O). CHS-1–GFP no longer accumulated at the Spk (P to S); as for CA treatment, several fluorescent crescent-shaped structures were observed in the apical and subapical regions immediately under the cell surface. Localization of CHS-1–GFP at septa was also disturbed (T and U) (white arrowhead). In addition, fluorescence was observed at the membrane of globular vacuoles (black arrowheads). Bars, 5 μm (500 μm in panel N).

plasm, we discovered a crucial difference in that each of these three chitin synthases is contained in a separate compartment, clearly resolved by simultaneous labeling with green and red fusion proteins. Most striking are the double-labeling images showing CHS-3 and CHS-1 as entirely separate populations of small particles. In the Spk, CHS-6 occupies a smaller area than CHS-1 and CHS-3. Earlier biochemical and cell fractionation studies on *S. cerevisiae* (19), *N. crassa* (20, 23), and other fungi had established the presence of CHS in chitosomes, a homogenous population

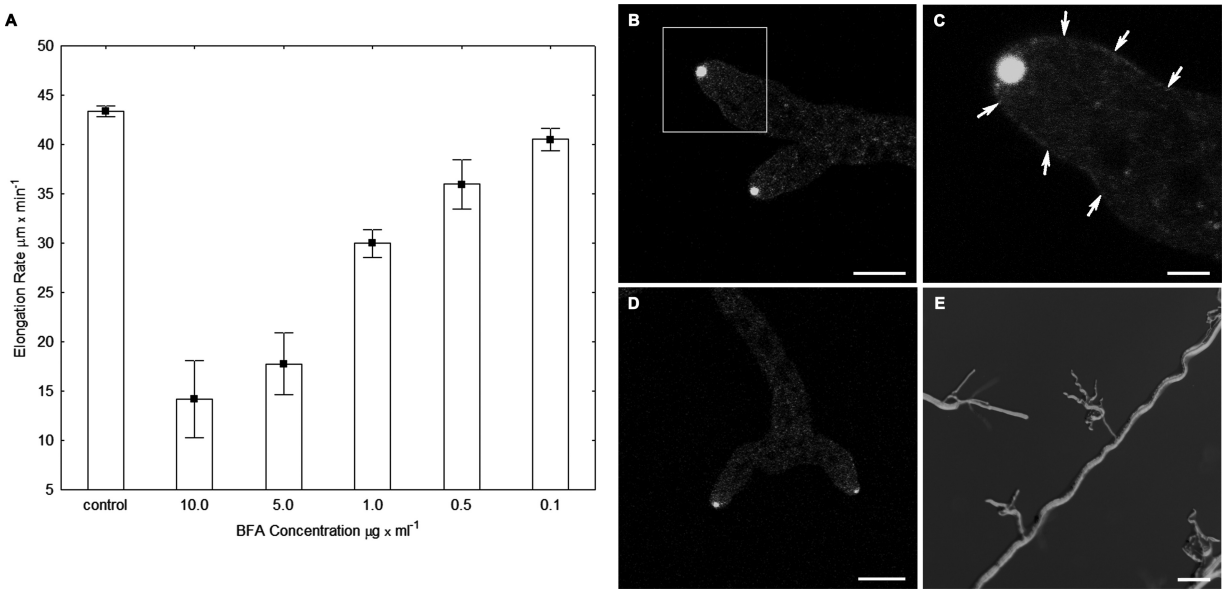

FIG. 9. Effect of brefeldin A (BFA) on the growth rate of *N. crassa* and in localization of CHS-1–GFP. Radial growth rate of *N. crassa* (n = 3) under different concentrations of BFA (A). LSCM analysis of hyphae of *N. crassa* strain NES2-11 exposed to BFA (5 μg/ml) (B to E). CHS-1–GFP was observed at the Spk of leading hyphae and branches of BFA-treated cells. Note how in some cells fluorescence occupied a larger Spk area than in untreated hyphae (B, inset). Accumulation of CHS-1–GFP fluorescence was also seen at the apical and subapical cell surface (C) (white arrows). Hyperbranching and dichotomous growth due to BFA effect were observed by LSCM (D) and bright-field microscopy (E). Bars, 10 μm (B and D), 2 μm (C), and 100 μm (E).

of microvesicles of low buoyant density, plus a less homogenous population of membranes of higher density. Although the actual size of the CHS-1–GFP fluorescent particles could not be ascertained from the confocal images, several studies of transmission electron microscopy of hyphal tips showed the presence of a population of microvesicles in the Spk core—the region where fluorescence is most intense. Hence, we conclude that some, if not most, of the fine fluorescent particles are microvesicles whose enzymatic cargo identified them as the previously characterized chitosomes. Collectively, our present data suggest the existence of different populations of chitosomes, each of them containing a class of CHSs, which eventually congregate at the apex within the Spk core. Further biochemical studies involving fractionation to separate specific subpopulations of chitosomes will be required to characterize these vesicles. In addition, studies on the remaining four other CHSs present in *N. crassa* are needed to show if they also are contained in discrete novel chitosome classes or are part of already-imaged chitosomes.

Another difference between the chitin synthases was the conspicuous accumulation of CHS-6 in subapical tubular vacuoles, a feature not observed for either CHS-1 or CHS-3. The finding of the three different CHSs in distal globular vacuoles and the observed retrograde movement of some vesicles (putative endosomes), plus the fact that endocytosis has been reported to occur mainly in the subapical regions of the hyphae (1, 38), lead us to suggest that the CHS-GFP released at the apex becomes, as the hypha grows, displaced to a subapical position, where it is endocytosed and transported to the vacuole for degradation.

Accumulation of CHS-1 to the Spk depends on an intact actin cytoskeleton. Benomyl had little effect on the delivery and distribution of CHS-1 at the Spk and septa, which strongly suggests that transport of CHS-1 is independent of the microtubular cytoskeleton. Conversely, under actin depolymerization conditions, CHS-1–GFP did not accumulate in the Spk but was found instead in subapical crescent-like structures close to the cell surface. This suggests that actin is necessary for Spk core assembly. A role of actin as scaffold regulating the distribution and stability of the Spk has been suggested. Accordingly, actin may be regulating the rate of vesicle flow, as deduced by the observation that the Spk in *Neurospora act-1* mutants was smaller than that in wild-type strains (40). Tropomyosin, an actin binding protein, and LifeAct labeled with fluorescent proteins were localized at the core of the Spk in hyphal tips of *N. crassa* (4, 11). In *Ustilago maydis*, mutations or deletion of the myosin motor-like domain (MMD) of Mcs1 (class V CHS) resulted in mislocalization, although not in loss of motility of Mcs1-GFP vesicles, suggesting that Mcs1 depends on a myosin-actin-based cytoskeleton for localization but requires MTs for motility (37). Unlike CHS classes V and VII, class III CHSs do not have any apparent MMDs and their mechanism of motility remains unknown. More studies are needed to investigate whether CHS-1 is transported along in chitosomes containing other CHSs with MMDs or is transported in another population of vesicles propelled by other motor proteins.

CHS-1 traffic is independent of the conventional ER-to-Golgi complex secretory pathway. The drug BFA has been traditionally used as an inhibitor of ER-to-Golgi complex traffic to study inhibition of the classical secretory pathway. BFA

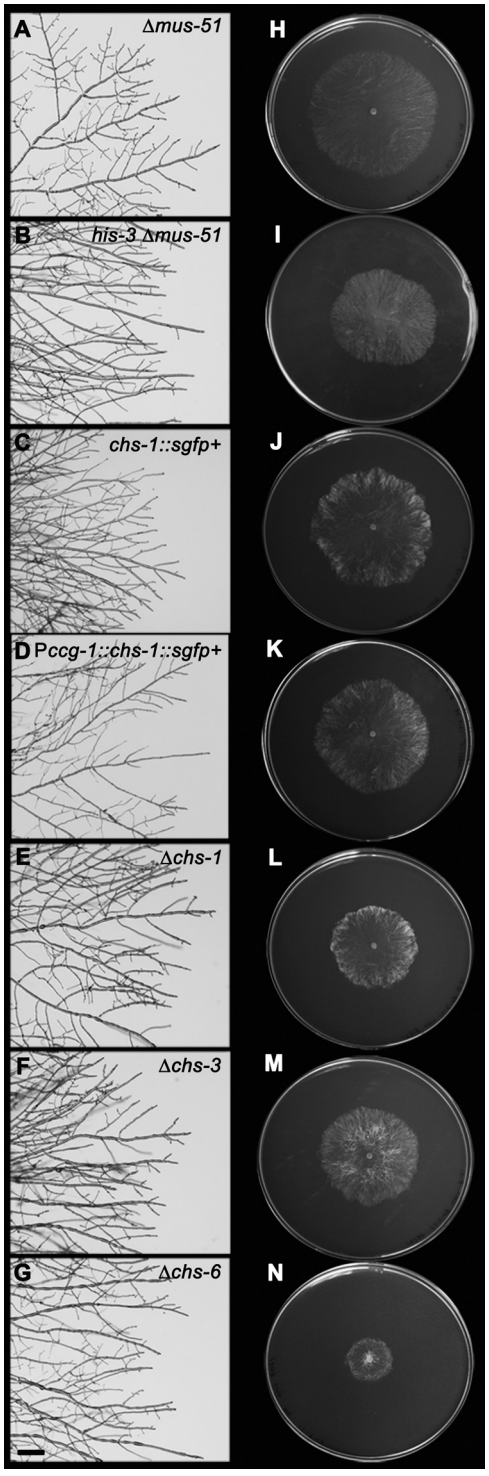

FIG. 10. Colony and hyphal morphology of the *N. crassa* strains analyzed in this study. Images of hyphae from the growing edges of the colonies of the different strains (A to G). Colony appearance after 24 h of growth under white light (H to N). Images correspond to the following strain genotypes: Δ*mus-51* (FGSC9718) (A and H), *his-3* Δ*mus-51* (FGSC9717) (B and I), *chs-1*::*sgfp*$^+$ (NES2-11) (C and J), P*ccg-1*::*chs-1*::*sgfp*$^+$ (NES1-15) (D and K), Δ*chs-1* (FGSC14318) (E and L), Δ*chs-3* (FGSC14320) (F and M), and Δ*chs-6* (FGSC13408) (G and N). Bar, 200 μm. Petri plates, 9 cm.

inhibits the membrane recruitment of the small GTPase ADP-ribosylation factor 1 (ARF1), one of the first steps in the formation of the coat protein complex I (COPI) that covers Golgi complex-derived vesicles (16). In filamentous fungi, as in mammalian cells, BFA leads to the disassembly of the Golgi complex equivalents and eventually to the arrest of apical extension (28). As the accumulation of CHS-1–GFP at the apex was not impeded by BFA, we suggest that the transport of CHS-1 may occur by an alternative nonconventional secretion pathway, as has been reported for some eukaryotic proteins (26). Similar results had been obtained with CHS-3 and CHS-6 (31). In addition, more intense and stable fluorescence was noticed in the Spk after BFA treatment, suggesting that a protein inhibited by BFA may be participating in the transport of CHS-containing vesicles from the Spk core to the plasma membrane, thus increasing the half-life of CHS-1–GFP in the Spk.

CHS-1 during germination. In contrast to the confocal images of well-developed hyphae, we failed to observe polarized distribution of CHS-1–GFP, CHS-3–GFP, or CHS-6–GFP during conidium germination and germ tube elongation. Earlier studies suggested either that young germ tubes (<12 h) did not contain chitin (glucosamine polymers) or that chitin was deposited at low densities in their cell walls (34). The latter explanation seems more plausible given that the growth rate of a germ tube is but a minuscule fraction of the growth rate of a mature hypha (2). In addition, transcriptional profiling data have shown that dormant conidia present minimal expression for 10 genes predicted to be involved in glucan and chitin synthesis and a peak expression at 0.5 h and afterwards (18). We did not see polarized expression of any of the GFP-tagged CHSs during conidial germination, but they were scattered through the cell, indicating that even though they are being synthesized, they are not being transported to the tip or not accumulating in sufficient quantities to be observed.

A role for class III chitin synthases? Class III CHSs are the only subfamily in division 1 of chitin synthases exclusively found in filamentous fungi (30). Previously, class III chitin synthase genes have been implicated in a variety of functions, including growth and pathogenicity. In *Coccidioides posadasii*, CpCHS3 appears more highly expressed during the saprobic mycelial phase than at stages of parasitic spherule development (22). Disruptants of *chs*B of *Aspergillus nidulans* grow as minute colonies, without conidia and with highly branched hyphae (5). In *A. nidulans* ChsB was localized at the tips of germ tubes, hyphal tips, and forming septa and during conidiogenesis (13). These authors showed that enhanced GFP (EGFP)-ChsB was distributed as a crescent in tips of germlings 60 to 70 μm in length and also during germination but coincided with the Spk in mature hyphae. In *Fusarium oxysporum*, no *chs3* mutants could be obtained, suggestive of the essential role of *chs3* for cell viability (24), and in *Botrytis cinerea* *Bcchs3*a has been reported to be involved in virulence (36). However, deletion of *CgChsIII* in *Colletotrichum graminicola* did not have obvious effects (42). Collectively, these data suggest that class III CHSs have undergone evolutionary divergence. The original *Neurospora chs-1* (class III) mutant, isolated after repeat-induced point mutation (RIP), exhibited aberrant morphology, hyphal swelling, thin aerial hyphae, deteriorated tips, scarce conidiation, and significant growth re-

duction, which suggested an important role of this enzyme in cell wall biosynthesis (44). In contrast, our examination of the Δ*chs-1* deletion mutant showed only a slight decrease in growth but, based on our unpublished data, a significant decrease in chitin synthase activity. One plausible explanation for these discrepancies is that *chs-1* mRNA synthesis was greatly reduced in the RIP strain but that likely some read-through occurred, generating CHS-1 protein with RIP-induced missense mutations, which are sufficiently severe to cause dominant synthetic effects. These effects are not expected to be obvious in a deletion strain because other CHS proteins can partially complement the complete lack of CHS-1.

CHS-1–GFP turnover. The generally accepted view is that chitin synthases operate at the cell surface presumably integrated into the plasma membrane. Yet, at the growing apex, we found only scant evidence of CHS-1 accumulation on the cell surface (apical plasma membrane). Conceivably, the density of CHS-1, as well as those of CHS-3 and CHS-6, positioned in action, may be too low to be easily detected in the membrane profiles, or alternatively, there may be a high rate of turnover after the CHSs reach their destination. On the other hand, accumulation of CHS-1–GFP, as well as of CHS-3 and CHS-6, can be clearly seen in the invaginating membrane during septum formation. Whereas CHS-3–GFP and CHS-6–GFP fluorescence disappeared about 20 min after septum completion (31), CHS-1–GFP fluorescence remained detectable for ~1 h after septum formation was completed. This suggests different half-lives for the three different enzymes, depending on their localization. Whether recycling or endocytosis explains the observed turnover remains an unexplored area in fungal biology.

Clues toward understanding cell wall synthesis. It is not clear if the horseshoe-shaped Spitzenring, composed of large secretory vesicles (macrovesicles), rotates around the Spk core or if a fraction of the peripheral macrovesicles are transiently lost. The last possibility is particularly exciting since the horseshoe-like structure could be the consequence of the delivery of secretory vesicles to the apical dome. Alternatively, both chitin synthases and glucan synthases could be delivered at different times, the horseshoe opening allowing the exit of CHS from the core to the cell surface. These observations suggest a spasmodic release of vesicles that could be related to the previously reported pulsed growth of *N. crassa* tips (21).

ACKNOWLEDGMENTS

We thank Michael Ferry and Stuart Brody (University of California San Diego) for the generous gift of the mCherry plasmid (pMFP24) and useful discussions. We are grateful to Alta Tecnología en Laboratorios SA de CV, Mexico, for the use of their Olympus microscopes and to Douglas Daniel (Arizona State University) for technical assistance with TIRF microscopy. We thank the Fungal Genetics Stock Center and the Neurospora Functional Genomics Program Project for materials and strains.

This work was supported by Consejo Nacional de Ciencia y Tecnología, Mexico (CONACYT, U-45818Q to M.R.) and by grants from the American Cancer Society (RSG-08-030-01-CCG to M.F.) and funds from NIH (ARRA supplement grant P01GM068087 to M.F.).

REFERENCES

1. **Araujo-Bazán, L., M. A. Peñalva, and E. A. Espeso.** 2008. Preferential localization of the endocytic internalization machinery to hyphal tips underlies polarization of the actin cytoskeleton in *Aspergillus nidulans*. Mol. Microbiol. **67:**891–905.
2. **Araujo-Palomares, C. L., E. Castro-Longoria, and M. Riquelme.** 2007. Ontogeny of the spitzenkörper in germlings of *Neurospora crassa*. Fungal Genet. Biol. **44:**492–503.
3. **Bartnicki-Garcia, S.** 1968. Cell wall chemistry, morphogenesis and taxonomy of fungi. Annu. Rev. Microbiol. **22:**87–107.
4. **Berepiki, A., A. Lichius, J.-Y. Shoji, J. Tilsner, and N. D. Read.** 2010. F-actin dynamics in *Neurospora crassa*. Eukaryot. Cell **9:**547–557.
5. **Borgia, P. T., et al.** 1996. The chsB gene of *Aspergillus nidulans* is necessary for normal hyphal growth and development. Fungal Genet. Biol. **20:**193–203.
6. **Borkovich, K. A., et al.** 2004. Lessons from the genome sequence of *Neurospora crassa*: tracing the path from genomic blueprint to multicellular organism. Microbiol. Mol. Biol. Rev. **68:**1–108.
7. **Bulawa, C. E.** 1993. Genetics and molecular biology of chitin synthesis in fungi. Annu. Rev. Microbiol. **47:**505–534.
8. **Bull, A. T.** 1970. Chemical composition of wild-type and mutant *Aspergillus nidulans* cell walls. The nature of polysaccharide and melanin constituents. J. Gen. Microbiol. **63:**75–94.
9. **Choquer, M., M. Boccara, I. R. Gonçalves, M. Soulié, and A. Vidal-Cros.** 2004. Survey of the *Botrytis cinerea* chitin synthase multigenic family through the analysis of six euascomycetes genomes. Eur. J. Biochem. **271:**2153–2164.
10. **Colot, H. V., et al.** 2006. A high-throughput gene knockout procedure for *Neurospora* reveals functions for multiple transcription factors. Proc. Natl. Acad. Sci. U. S. A. **13:**10352–10357.
11. **Delgado-Alvarez, D. L., et al.** 2010. Visualization of F-actin localization and dynamics with live cell markers in *Neurospora crassa*. Fungal Genet. Biol. **47:**573–586.
12. **Freitag, M., P. C. Hickey, N. B. Raju, E. U. Selker, and N. D. Read.** 2004. GFP as a tool to analyze the organization, dynamics and function of nuclei and microtubules in *Neurospora crassa*. Fungal Genet. Biol. **41:**897–910.
13. **Fukuda, K., et al.** 2009. Class III chitin synthase ChsB of *Aspergillus nidulans* localizes at the sites of polarized cell wall synthesis and is required for conidial development. Eukaryot. Cell **8:**945–956.
14. **Galagan, J. E., et al.** 2003. Genome sequence of the filamentous fungus *Neurospora crassa*. Nature **422:**859–868.
15. **Glaser, L., and D. H. Brown.** 1957. The synthesis of chitin in cell free extracts of *Neurospora crassa*. J. Biol. Chem. **228:**729–742.
16. **Helms, J. B., and J. E. Rothman.** 1992. Inhibition by brefeldin A of a Golgi membrane enzyme that catalyses exchange of guanine nucleotide bound to ARF. Nature **360:**352–354.
17. **Hickey, P. C., S. M. Swift, M. G. Roca, and N. D. Read.** 2005. Live-cell imaging of filamentous fungi using vital fluorescent dyes. Methods Microbiol. **34:**63–87.
18. **Kasuga, T., et al.** 2005. Long-oligomer microarray profiling in *Neurospora crassa* reveals the transcriptional program underlying biochemical and physiological events of conidial germination. Nucleic Acids Res. **33:**6469–6485.
19. **Leal-Morales, C., C. E. Bracker, and S. Bartnicki-Garcia.** 1988. Localization of chitin synthase in cell-free homogenates of *Saccharomyces cerevisiae*: chitosomes and plasma membrane. Proc. Natl. Acad. Sci. U. S. A. **85:**8516–8520.
20. **Leal-Morales, C. A., C. E. Bracker, and S. Bartnicki-Garcia.** 1994. Subcellular localization, abundance and stability of chitin synthetases 1 and 2 from *Saccharomyces cerevisiae*. Microbiology **140:**2207–2216.
21. **Lopez-Franco, R., S. Bartnicki-Garcia, and C. E. Bracker.** 1994. Pulsed growth of fungal hyphal tips. Proc. Natl. Acad. Sci. U. S. A. **91:**12228–12232.
22. **Mandel, M. A., J. N. Galgiani, S. Kroken, and M. J. Orbach.** 2006. *Coccidioides posadasii* contains single chitin synthase genes corresponding to classes I to VII. Fungal Genet. Biol. **43:**775–788.
23. **Martinez, J. P., G. Gimenez, C. E. Bracker, and S. Bartnicki-Garcia.** 1989. Sedimentation properties of chitosomal chitin synthetase from the wild-type strain and the 'slime' variant of *Neurospora crassa.* Biochim. Biophys. Acta **990:**45–52. (Erratum, **1073:**239, 1991.)
24. **Martín-Udíroz, M., M. P. Madrid, and M. I. G. Roncero.** 2004. Role of chitin synthase genes in *Fusarium oxysporum*. Microbiol. Mol. Biol. Rev. **150:**3175–3187.
25. **Mourino-Perez, R. R., R. W. Roberson, and S. Bartnicki-Garcia.** 2006. Microtubule dynamics and organization during hyphal growth and branching in *Neurospora crassa*. Fungal Genet. Biol. **43:**389–400.
26. **Nickel, W.** 2005. Unconventional secretory routes: direct protein export across the plasma membrane of mammalian cells. Traffic **6:**607–614.
27. **Ninomiya, Y., K. Suzuki, C. Ishii, and H. Inoue.** 2004. Highly efficient gene replacements in *Neurospora* strains deficient for nonhomologous end-joining. Proc. Natl. Acad. Sci. U. S. A. **101:**12248–12253.
28. **Pantazopoulou, A., and M. A. Penalva.** 2009. Organization and dynamics of the *Aspergillus nidulans* golgi during apical extension and mitosis. Mol. Biol. Cell **20:**4335–4347.
29. **Read, N. D., and P. C. Hickey.** 2001. The vesicle trafficking network and tip growth in fungal hyphae, p. 137–146. *In* A. Geitmann, M. Cresti, and I. B. Heath (ed.), Cell biology of plant and fungal tip growth. IOS Press, Amsterdam, Netherlands.
30. **Riquelme, M., and S. Bartnicki-García.** 2008. Advances in understanding hyphal morphogenesis: ontogeny, phylogeny and cellular localization of chitin synthases. Fungal Biol. Rev. **22:**56–70.
31. **Riquelme, M., et al.** 2007. Spitzenkörper localization and intracellular traffic

of green fluorescent protein-labeled CHS-3 and CHS-6 chitin synthases in living hyphae of *Neurospora crassa*. Eukaryot. Cell **6:**1853–1864.
32. **Riquelme, M., C. G. Reynaga-Pena, G. Gierz, and S. Bartnicki-Garcia.** 1998. What determines growth direction in fungal hyphae? Fungal Genet. Biol. **24:**101–109.
33. **Ruiz-Herrera, J., C. G. Leon, A. Carabez-Trejo, and E. Reyes-Salinas.** 1996. Structure and chemical composition of the cell walls from the haploid yeast and mycelial forms of *Ustilago maydis*. Fungal Genet. Biol. **20:**133–142.
34. **Schmit, J. C., C. M. Edson, and S. Brody.** 1975. Changes in glucosamine and galactosamine levels during conidial germination in *Neurospora crassa*. J. Bacteriol. **122:**1062–1070.
35. **Schoffelmeer, E. A. M., F. M. Klis, J. H. Sietsma, and B. J. C. Cornelissen.** 1999. The cell wall of *Fusarium oxysporum*. Fungal Genet. Biol. **27:**275–282.
36. **Soulié, M. C., et al.** 2006. *Botrytis cinerea* virulence is drastically reduced after disruption of chitin synthase class III gene (Bcchs3a). Cell. Microbiol. **8:**1310–1321.
37. **Treitschke, S., G. Doehlemann, M. Schuster, and G. Steinberg.** 2010. They myosin motor domain of fungal chitin synthase V is dispensable for vesicle motility but required for virulence of the maize pathogen *Ustilago maydis*. Plant Cell **22:**2476–2494.
38. **Upadhyay, S., and B. D. Shaw.** 2008. The role of actin, fimbrin and endocytosis in growth of hyphae in *Aspergillus nidulans*. Mol. Microbiol. **68:**690–705.
39. **Verdín, J., S. Bartnicki-Garcia, and M. Riquelme.** 2009. Functional stratification of the Spitzenkörper of *Neurospora crassa*. Mol. Microbiol. **74:**1044–1053.
40. **Virag, A., and A. J. Griffiths.** 2004. A mutation in the *Neurospora crassa* actin gene results in multiple defects in tip growth and branching. Fungal Genet. Biol. **41:**213–225.
41. **Vogel, H. J.** 1956. A convenient growth medium for *Neurospora* (medium N). Microbiol. Gen. Bull. **13:**42–43.
42. **Werner, S., J. A. Sugui, G. Steinberg, and H. B. Deising.** 2007. A chitin synthase with a myosin-like motor domain is essential for hyphal growth, appressorium differentiation, and pathogenicity of the maize anthracnose fungus *Colletotrichum graminicola*. Mol. Plant Microbe Interact. **20:**1555–1567.
43. **Westergaard, M., and H. K. Mitchell.** 1942. *Neurospora* V. A synthetic medium favoring sexual reproduction. Am. J. Bot. **14:**573–577.
44. **Yarden, O., and C. Yanofsky.** 1991. Chitin synthase 1 plays a major role in cell wall biogenesis in *Neurospora crassa*. Genes Dev. **5:**2420–2430.